



Divergent white matter changes in patients with nasopharyngeal carcinoma post-radiotherapy with different outcomes: a potential biomarker for prediction of radiation necrosis

Xiaoshan Lin¹ · Zhipeng Li² · Shengli Chen¹ · Yadi Yang² · Haoqiang He² · Xiaofei Lv² · Yingwei Qiu¹

Received: 29 December 2021 / Revised: 17 May 2022 / Accepted: 23 May 2022 / Published online: 10 June 2022

© The Author(s), under exclusive licence to European Society of Radiology 2022, corrected publication 2022

Abstract

Objectives To investigate the effects of standard radiotherapy on temporal white matter (WM) and its relationship with radiation necrosis (RN) in patients with nasopharyngeal carcinoma (NPC), and to determine the predictive value of WM volume alterations at the early stage for RN occurrence at the late-delay stage.

Methods Seventy-four treatment-naive NPC patients treated with standard radiotherapy were longitudinally followed up for 36 months. Structural MRIs were collected at multiple time points during the first year post-radiotherapy. Longitudinal structural images were processed using FreeSurfer. Linear mixed models were used to delineate divergent trajectories of temporal WM changes between patients who developed RN and who did not. Four machine learning methods were used to construct predictive models for RN with temporal WM volume alterations at early-stage.

Results The superior temporal gyrus (STG) had divergent atrophy trajectories in NPC patients with different outcomes (RN vs. NRN) post-radiotherapy. Patients with RN showed more rapid atrophy than those with NRN. A predictive model constructed with temporal WM volume alterations at early-stage post-radiotherapy had good performance for RN; the areas under the curve (AUC) were 0.879 and 0.806 at 1–3 months and 6 months post-radiotherapy, respectively. Moreover, the predictive model constructed with absolute temporal volume at 1–3 months post-radiotherapy also presented good performance; the AUC was 0.842, which was verified by another independent dataset (AUC = 0.773).

Conclusions NPC patients with RN had more sharp atrophy in the STG than those with NRN. Temporal WM volume at early-stage post-radiotherapy may serve as an in vivo biomarker to identify and predict RN occurrence.

Key Points

- The STG had divergent atrophy trajectories in NPC patients with different outcomes (RN vs. NRN) post-radiotherapy.
- Although both groups exhibited time-dependent atrophy in the STG, the patients with RN showed a more rapid volume decrease than those with NRN.
- Temporal WM volume alteration (or absolute volume) at the early stage could predict RN occurrence at the late-delay stage after radiotherapy.

Xiaoshan Lin and Zhipeng Li contributed equally to this work.

✉ Xiaofei Lv
lvxf@sysucc.org.cn

✉ Yingwei Qiu
qiuyw1201@gmail.com

¹ Department of Radiology, Huazhong University of Science and Technology Union Shenzhen Hospital, Shenzhen 518052, China

² Department of Medical Imaging, Sun Yat-sen University Cancer Center, State Key Laboratory of Oncology in South China, Collaborative Innovation Center for Cancer Medicine, Guangdong Key Laboratory of Nasopharyngeal Carcinoma Diagnosis and Therapy, Guangzhou 510060, China

Keywords Radiotherapy · Nasopharyngeal carcinoma · Radiation-induced temporal lobe necrosis · White matter · Machine learning

Abbreviations

AJCC	American Joint Committee on Cancer
AUC	Area under the curve
BANKSSTS	Banks of the superior temporal sulcus
DKI	Diffusion kurtosis imaging
FUS	Fusiform
GM	Gray matter
IMRT	Intensity-modulated radiation therapy
ITG	Inferior temporal gyrus
KNN	k-nearest neighbors
LMM	Linear mixed model

LR	Logistic regression
MRI	Magnetic resonance imaging
MTG	Middle temporal gyrus
NPC	Nasopharyngeal carcinoma
PHG	Parahippocampal gyrus
RF	Random forest
RN	Radiation-induced temporal lobe necrosis
ROC	Receiver operating characteristic
RT	Radiotherapy
RTL	Radiation-induced temporal lobe injury
SMG	Supramarginal gyrus
STG	Superior temporal gyrus
SVM	Support vector machine
TP	Temporal pole
TTG	Transverse temporal gyrus
WM	White matter

Introduction

Nasopharyngeal carcinoma (NPC) is a malignant head and neck cancer prevalent in southern China, especially in Guangdong and Guangxi Province [1, 2]. Radiotherapy (RT) with or without adjuvant chemotherapy remains the primary treatment for NPC due to its radiosensitivity [3, 4]. However, owing to the proximity to the RT target area, radiation-induced temporal lobe necrosis (RN) is a common late neurological complication, with an incidence of 4.6–8.5% according to a previous report [5]. Evidence has shown that RN is permanent, irreversible, and may progress with time [6, 7], which would cause a series of neurological symptoms, such as memory loss, cognitive impairment, dysfunction in attention and visual perception, thereby severely affecting the patients' quality of life [8, 9]. Thus, accurate prediction of RN at the acute or early-delay stage post-RT (less than 6 months post-RT, which is reversible) would be helpful. Recent reports have indicated that RT-related brain alterations at the early stage are the warning signs of neurocognitive dysfunction at the late-delay stage post-RT [10–14]. However, whether RT-related brain alterations at the early stage can be used to predict RN at the late-delay stage is still an open question. Therefore, the knowledge of the longitudinal evolution of brain structure changes from the acute stage to the late-delay stage in patients with NPC post-RT and its relationship with RN is of great significance for the early identification and prevention of RN.

Cerebral white matter (WM) has been reported to be more susceptible to radiation damage than gray matter (GM), which may be attributed to the relative scarcity of the blood supply to the WM [15, 16]. Increasing evidence has shown that RT-related WM microstructural changes and WM volumetric alterations are potential biomarkers of radiation brain injury [10, 11, 17–19]. More recently, studies have indicated that early RT-related WM microstructural destruction plays a potential predictive role for late-delay stage RN [20, 21]. Using diffusion

kurtosis imaging (DKI), Lu et al retrospectively evaluated the early diffusion and kurtosis features of temporal WM in patients with NPC who developed RN. Their results showed that the mean kurtosis decreased significantly at 4 weeks during RT and 1 month after RT, which may represent a valuable early indicator of RT-induced WM microstructural damage to the temporal lobe [20]. However, to date, limited studies have assessed the significance of RT-related WM volumetric alterations in the detection of RN, which is easier to obtain in clinical practice than diffusion [19, 22]. Our previous study showed that patients with NPC had time- and dose-dependent WM atrophy in selective subfields of the temporal lobe after RT compared to healthy controls [23]; however, the relationship between this time- and dose-dependent WM atrophy and RN remains unclear. Therefore, we attempted to further investigate whether RT-related temporal WM volumetric alterations at the early stage could serve as an imaging marker for RN at the late-delay stage.

Machine learning has been widely used in medical imaging, and it can extract meaningful patterns from imaging data with different algorithms to classify and predict at the individual level [24, 25]. In this study, we aimed (1) to delineate the divergent patterns of longitudinal WM volumetric alterations in patients with NPC between those who developed RN and those who did not, and (2) to construct a predictive model for RN with WM volumetric alterations at the early stage post-RT with machine learning methods.

Materials and methods

Participants

Between December 2014 and August 2018, 150 treatment-naive patients with NPC were recruited, and they underwent baseline magnetic resonance imaging (MRI). All patients had been pathologically confirmed, and the clinical stage of each patient was defined according to the American Joint Committee on Cancer System (7th edition); thereafter, all patients received standard RT at the Sun Yat-sen University Cancer Center (Guangzhou, China). Seventy-four of these patients (aged 18–55 years, 46 males and 28 females) who completed at least 36 months follow-up and had at least one MRI at 1–3 or 6 months post-RT (some also had MRI at 9–12 months post-RT) were finally enrolled in the present study. The details of the inclusion criteria are presented in the [Supplementary Materials](#). During the follow-up period, 15 patients developed RN, which was confirmed through repeated MRI follow-ups and were classified as the RN group, while 59 patients who did not develop RN were classified as the NRN group. The procedures for the enrollment and follow-up of the participants are illustrated in Fig. 1. The clinical data of each patient in the RN group are summarized in Table 1, and the distribution of necrotic lesions is shown in Fig. 2. In addition to the baseline (pre-RT) MRI collected from all

Table 1 Clinical data of the patients in the RN group

Patient	Time to RN after RT (months)	Site of necrosis	Clinical stage (AJCC)
1	36	Right temporal lobe	T4N2M0 IVa
2	24	Left temporal lobe	T4N1M0 IV
3	14	Right temporal lobe	T4N1M0 Iva
4	27	Right temporal lobe	T4N1M0 Iva
5	12	Right temporal lobe	T3N2M0 III
6	24	Right temporal lobe	T3N2M0 III
7	24	Left temporal lobe	T4N2M0 IVa
8	18 / 25	Left / Right temporal lobe	T3N2M0 III
9	28	Left temporal lobe	T4N2M0 IVa
10	12 / 12	Left / Right temporal lobe	T4N3M0 IVb
11	5 / 5	Left / Right temporal lobe	T4N2M1 IVc
12	20 / 20	Left / Right temporal lobe	T4N2M0 Iva
13	33	Right temporal lobe	T4N1M0 IV
14	19	Right temporal lobe	T4N1M0 Iva
15	7 / 13	Right / Left temporal lobe	T4N1M0 Iva

Abbreviations: *RN*, radiation-induced temporal lobe necrosis; *RT*, radiotherapy; *AJCC*, American Joint Committee on Cancer

patients, 68 patients had a follow-up MRI within 3 months post-RT, 54 patients had a follow-up MRI at 6 months post-RT, and 31 patients had a follow-up MRI at 9–12 months post-RT; thus, 227 MRI datasets were finally collected. This study was approved by the local Institutional Review Board, and written informed consent was obtained from all participants.

Treatment

All NPC patients were treated with intensity-modulated radiation therapy (IMRT) ($n = 69$) or tomography radiation therapy ($n = 5$) at the Sun Yat-sen University Cancer Center. The prescribed regimen included a total dose of 68–70 Gy in 30–33 fractions at 2.12–2.33 Gy/fraction to the planning target volume (PTV) of the primary gross tumor volume (GTV_{nx}), 60–70 Gy to the PTV of the GTV of involved lymph nodes (GTV_{nd}), 60–64 Gy to the PTV of the high-risk clinical target volume (CTV1), and 54–58 Gy to the PTV of the low-risk clinical target volume (CTV2). Details are presented in the [Supplementary Materials](#).

Dosimetric evaluation for the bilateral temporal lobes

The bilateral temporal lobes were manually delineated on treatment planning CT axial images by referring to T1-weighted anatomical imaging, and the dose-volume statistics for the temporal lobes were calculated. Dose evaluation was performed based on the data from the dose-volume histogram for the targets. The main evaluation parameters were maximum dose (D_{max}), mean dose (D_{mean}), and minimum dose (D_{min}) received by temporal tissues. Dose-volume statistics of the temporal lobe in the RN group and the NRN group are listed in [Supplementary Table 1](#).

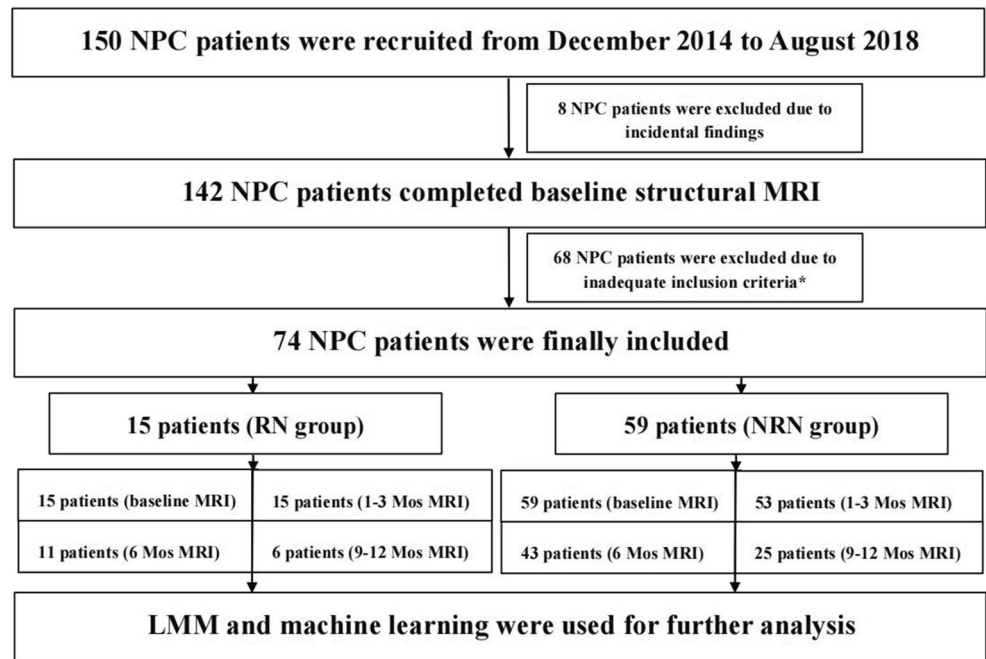
MRI acquisition

We collected MRI data with a GE Discovery MR 750 3.0-T scanner (GE Medical Systems) using a 16-channel head and neck coil at the Department of Medical Imaging, Sun Yat-sen University Cancer Center. Conventional MRI sequences, including axial T1-weighted and T2-weighted images, T2-FLAIR images, and contrast-enhanced T1-weighted images, were acquired to rule out intraparenchymal invasion and to detect RN during follow-up. Additionally, high-resolution structural MRI scans with T1-weighted three-dimensional brain volume imaging (3D-BRAVO) were obtained for volumetric evaluation. The scanning parameters were as follows: TR = 8.16 ms, TE = 3.18 ms, TI = 800 ms, flip angle = 8°, acquisition matrix = 256 × 256, field of view = 256 × 256 mm², and voxel size = 1 × 1 × 1 mm³.

Image processing

Structural images were processed using the open-source FreeSurfer pipeline (version 6.0, <http://surfer.nmr.mgh.harvard.edu>). The processing procedure mainly included skull removal, B1 bias field correction, data registration, and gray-white matter segmentation [26]. Finally, 11 subfields of the temporal lobe were extracted using an automated FreeSurfer segmentation script, and the WM volumetric values of these regions were subsequently measured. The 11 subfields included banks of the superior temporal sulcus (BANKSSTS), fusiform (FUS), inferior temporal gyrus (ITG), middle temporal gyrus (MTG), parahippocampal gyrus (PHG), pars opercularis, superior temporal gyrus (STG),

Fig. 1 Enrollment and follow-up procedures for patients with NPC. *Forty-eight patients did not complete at least a 36-month follow-up, and 20 patients did not have at least one MRI at 1-3 or 6 months post-RT during the follow-up. Abbreviations: Mos, months; NPC, nasopharyngeal carcinoma; RT, radiotherapy; RN, radiation-induced temporal lobe necrosis; LMM, linear mixed model



supramarginal gyrus (SMG), temporal pole (TP), transverse temporal gyrus (TTG), and insular gyrus.

Statistical analysis

All analyses were conducted with the open-source R software (version 4.0.2).

Demographic analysis

Two-sample independent t-test was performed to evaluate the age and education level differences between the two groups at baseline. Pearson’s chi-squared test was applied to assess the differences in gender and treatment between the two groups at baseline. Differences with a *p* value < 0.05 (two-sided) were considered statistically significant.

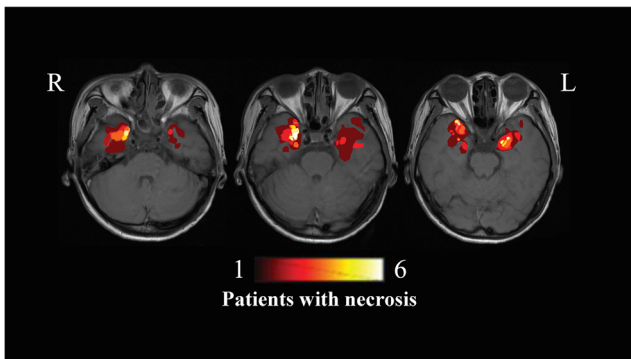


Fig. 2 Density distribution maps showing the overlap of necrotic lesions in the full sample of 15 patients in the RN group. Abbreviations: RN, radiation-induced temporal lobe necrosis

Longitudinal temporal WM volume trajectories in patients with NPC post-RT

To reduce the individual differences, we standardized the WM volume of each patient at each time point during follow-up by dividing by their baseline data. Additionally, in five patients with NPC in the RN group who had necrotic lesions on both sides of the temporal lobes, we treated the unilateral temporal lobe as one sample, thus forming 20 samples. For patients in the NRN group, as no differences were found between the left and right sides (Supplementary Table 2), the WM volumes of the 11 subfields of temporal lobes were bilaterally averaged, thus forming 59 samples.

Given that our previous studies have shown that the RT-associated morphological alterations in patients with NPC are linear [14, 19], linear mixed models (LMM) were used to evaluate the longitudinal changes in WM volume of the subfields of temporal lobes, which modeled fixed and random effects simultaneously and accounted for unequal sampling intervals and missing data [27, 28]. First, to explore whether the WM volume underwent different changes post-RT between the two groups, we modeled the first LMM (model 1) with an interaction effect between groups (RN and NRN group) and time (in months):

$$\begin{aligned}
 Y_{ij} = & \gamma_{00} + \gamma_{01}(treatment_j) + \gamma_{02}(group_j) \\
 & + \gamma_{10}(time_i_j) + \gamma_{11}(group_j \times time_i_j) + \mu_{0j} \\
 & + \mu_{1j}(time_i_j) + r_{ij} \text{ (Model 1)}
 \end{aligned}
 \tag{1}$$

where Y_{ij} denotes WM volume for the j th participant on the i th follow-up visit after RT, and the longitudinal variable represents the time interval after completion of RT. The pretreatment session with the quality structural MRI data of each participant was defined as the baseline. Time always started from zero. The longitudinal time-dependent effect was expressed as a simple regression between time and Y with residual r . Group (RN or NRN group) and treatment (with or without neoadjuvant chemotherapy) were binary dummy variables.

Then, for the selective subfields that showed significantly different longitudinal changes in WM volume between groups, we examined the longitudinal changes in the two groups separately via the following second LMM:

$$Y_{ij} = \gamma_{00} + \gamma_{01}(\text{treatment}_j) + \gamma_{10}(\text{time}_{ij}) + \mu_{0j} + \mu_{1j}(\text{time}_{ij}) + r_{ij}(\text{Model 2}) \quad (2)$$

where the variables are the same as those in model 1. To address the multiple testing for the various hypotheses, the Holm-Bonferroni method was applied for controlling family-wise errors at an alpha level of 0.05.

Construction of prediction models for RN with temporal WM volume alterations at the early stage post-RT

First, to reduce the difference in dimensions and value ranges between features, we standardized the data and mapped the values to [0, 1] through min-max normalization. Next, the WM volumes of the 11 subfields of temporal lobes at the early stage (1–3 months and 6 months post-RT) were used as structural features, of which the relatively prominent features were extracted by the Boruta package embedded in the R software, and then, machine learning methods were used to construct the prediction models. The RN and NRN groups were randomly sorted into the training set and testing set at a ratio of 7:3. Four machine learning methods, namely support vector machine (SVM), logistic regression (LR), random forest (RF),

and k-nearest neighbors (KNN), were used to construct prediction models for RN with temporal WM alterations at the early stage; age and dose were also included as factors in the models. With 10-fold cross-validation, receiver operating characteristic (ROC) curves and the corresponding area under the curve (AUC) values were used to evaluate the diagnostic efficiency of different models. Based on the best diagnostic threshold, the accuracy, sensitivity, and specificity were calculated. Moreover, we constructed two additional prediction models with dosimetric factor and temporal WM volume only to compare their independent predictive values. DeLong tests were used to assess the differences in the ROC curves.

Construction of prediction models for RN with absolute temporal WM volume at the early stage post-RT and verified in another independent dataset

In addition to temporal WM volume alteration, we constructed prediction models for RN with absolute temporal WM volume (which is more easily obtained in clinical practice) at 1–3 months post-RT using similar methods to those presented in the “Construction of prediction models for RN with temporal WM volume alterations at the early stage post-RT.” We verified the models with another independent dataset; detailed information on the independent dataset is presented in the [Supplementary Materials](#).

Results

Demographic and clinical data at baseline

The demographic characteristics of the RN group and the NRN group at baseline are presented in Table 2. There were no significant differences in age (40.47 ± 7.73 years for RN, 38.25 ± 9.46 years for NRN; $p = 0.41$), gender (8 males and 7 females for RN, 38 males and 21 females for NRN; $p = 0.43$), education level (10.53 ± 3.64 years for RN, 12.22 ± 3.03 years for NRN; p

Table 2 Demographic characteristics of the RN group and NRN group at baseline

Demographic information	RN group ($N = 15$)	NRN group ($N = 59$)	t / χ^2 values	p values
Age (years)*	40.47 ± 7.73	38.25 ± 9.46	0.84	0.41
Education (years)*	10.53 ± 3.64	12.22 ± 3.03	−1.85	0.07
Gender (M/F)#	8/7	38/21	0.62	0.43
Treatment (with/without neoadjuvant chemotherapy)#	10/5	28/31	1.77	0.18
AJCC stage (I/II/III/IV)#	0/0/3/12	1/7/34/17	NA	NA

*Data are presented as mean \pm standard deviation. # Data are shown in numbers

Abbreviations: RN, radiation-induced temporal lobe necrosis; NRN, no radiation-induced temporal lobe necrosis; M/F, male/female; AJCC, American Joint Committee on Cancer; N, number; NA, not available

Table 3 Longitudinal RT-related WM atrophy in the STG in the RN group and the NRN group. Statistically significant effects ($p < 0.05$) appear in bold (corrected for multiple comparisons, $p < 0.0045$ for all the 11 parcels)

Group	Predictor	Coefficient	Standard error	<i>t</i>	<i>p</i>
RN group	Treatment	- 2.52E-03	6.16E-03	- 0.41	0.68
	Time post-RT (months)	- 2.90E-03	8.05E-04	- 3.61	< 0.001*
NRN group	Treatment	- 8.87E-04	2.30E-03	- 0.39	0.70
	Time post-RT (months)	- 9.52E-04	2.91E-04	- 3.27	0.001*

Abbreviations: *RT*, radiotherapy; *WM*, white matter; *STG*, superior temporal gyrus; *RN*, radiation-induced temporal lobe necrosis; *NRN*, no radiation-induced temporal lobe necrosis

= 0.07), and treatment (10 patients with neoadjuvant chemotherapy and 5 patients without neoadjuvant chemotherapy for RN, 28 patients with neoadjuvant chemotherapy and 31 patients without neoadjuvant chemotherapy for NRN; $p = 0.18$) between the two groups at baseline.

$p = 0.004$) (Fig. 3a, Supplementary Table 3). Although both groups exhibited time-dependent WM atrophy in the STG in the first year post-RT, the RN patients ($\beta_{\text{Time}} = -2.90 \times 10^{-3}$, $p < 0.001$) showed more rapid atrophy than those in the NRN group ($\beta_{\text{Time}} = -9.52 \times 10^{-4}$, $p = 0.001$) (Table 3 and Fig. 3b, c).

Divergent trajectories of temporal WM volume changes in the RN and NRN groups within 1-year post-RT

Temporal WM volume alterations at the early stage post-RT could predict RN occurrence in patients with NPC during 36 months of follow-up

Significant different trajectories were observed in the STG between the RN and NRN groups ($\beta_{\text{Time*Group}} = 1.98 \times 10^{-3}$,

WM volumetric alterations in the TP, FUS, BANKSSTS, MTG, STG, SMG, and ITG at 1–3 months post-RT and

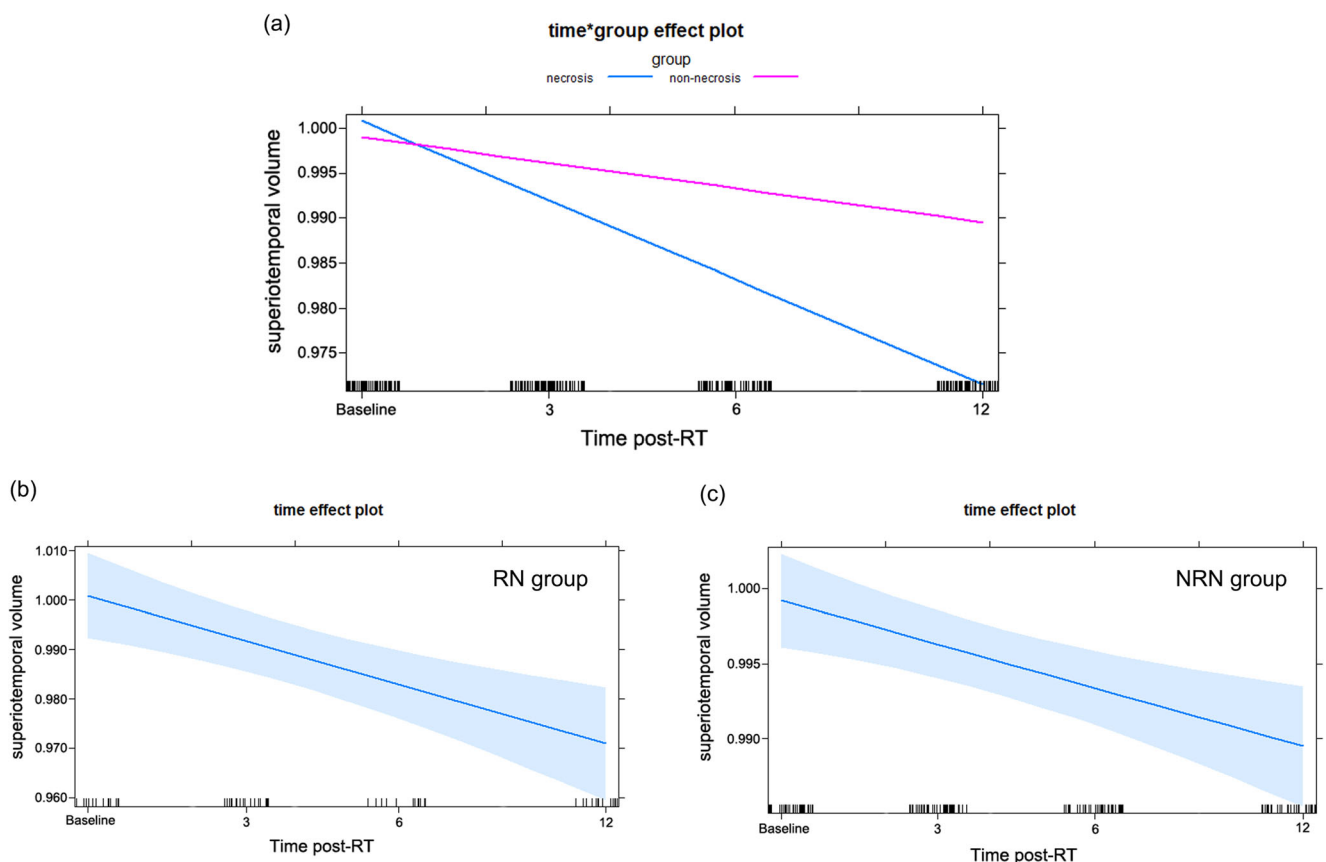


Fig. 3 Longitudinal WM volume alterations in the STG within 1-year post-RT. **a** Different trajectories of the WM volume in the RN group and NRN group. **b** Longitudinal WM volume alterations in the RN group. **c** Longitudinal WM volume alterations in the NRN group.

Abbreviations: WM, white matter; STG, superior temporal gyrus; RT, radiotherapy; RN, radiation-induced temporal lobe necrosis; NRN, no radiation-induced temporal lobe necrosis

Table 4 Predictive efficiency for RN with temporal WM volume alteration at 1–3 months and 6 months in NPC patients post-RT based on different machine learning methods

	Model	Testing Set			
		AUC	Accuracy	Sensitivity	Specificity
1–3 months	SVM	0.879	0.778	0.714	0.800
	LR	0.853	0.833	0.800	0.842
	RF	0.719	0.818	0.750	0.833
	KNN	0.725	0.875	0.667	0.905
6 months	SVM	0.806	0.818	0.750	0.833
	LR	0.800	0.842	0.800	0.857
	RF	0.767	0.833	0.500	0.929
	KNN	0.664	0.789	0.667	0.813

Abbreviations: *RN*, radiation-induced temporal lobe necrosis; *WM*, white matter; *NPC*, nasopharyngeal carcinoma; *RT*, radiotherapy; *SVM*, support vector machine; *LR*, logistic regression; *RF*, random forest; *KNN*, k-nearest neighbors; *AUC*, area under the curve

WM volumetric alterations in the BANKSSTS, insular gyrus, and TP at 6 months post-RT had important characteristic attributes (Fig. 4), which were used to construct the prediction models. All models constructed with different machine learning methods (SVM, LR, RF, and KNN) showed acceptable predictive power (AUC = 0.879, 0.853, 0.719 and 0.725, accuracy = 0.778, 0.833, 0.818, and 0.875 for SVM, LR, RF and KNN at 1–3 months post-RT, respectively; AUC = 0.806, 0.800, 0.767, and 0.664, accuracy = 0.818, 0.842, 0.833, and 0.789 for SVM, LR, RF, and KNN at 6 months post-RT, respectively), while the prediction model constructed by

SVM had the best diagnostic performance on the testing set verification (Table 4 and Fig. 5). The AUC value, accuracy, sensitivity, and specificity were 0.879, 0.778, 0.714, and 0.800, respectively at 1–3 months post-RT, while the AUC value, accuracy, sensitivity, and specificity were 0.806, 0.818, 0.750, and 0.833 at 6 months post-RT, respectively.

Moreover, based on the SVM, the result of the prediction model constructed with only the temporal WM volume at 1–3 months post-RT showed an AUC value, accuracy, sensitivity, and specificity of 0.841, 0.733, 0.750, and 0.727, respectively, while the result of the prediction model constructed with only the dosimetric factor showed an AUC value, accuracy, sensitivity, and specificity of 0.789, 0.783, 0.500, and 0.842, respectively (Supplementary Figure 2). Furthermore, we found the model constructed with both the temporal WM volume at 1–3 months post-RT and the dosimetric factor performed better than the model constructed with only the temporal WM volume at 1–3 months post-RT ($p = 0.04$) and also performed better than the model constructed with only the dosimetric factor ($p < 0.001$), while the model constructed with only the temporal WM volume at 1–3 months post-RT performed better than the model constructed with only the dosimetric factor ($p = 0.01$).

Absolute temporal WM volume at the early stage post-RT could also predict RN occurrence in patients with NPC during 36 months of follow-up, which was verified in another independent dataset

Interestingly, prediction models constructed with absolute temporal volume at 1–3 months post-RT also presented

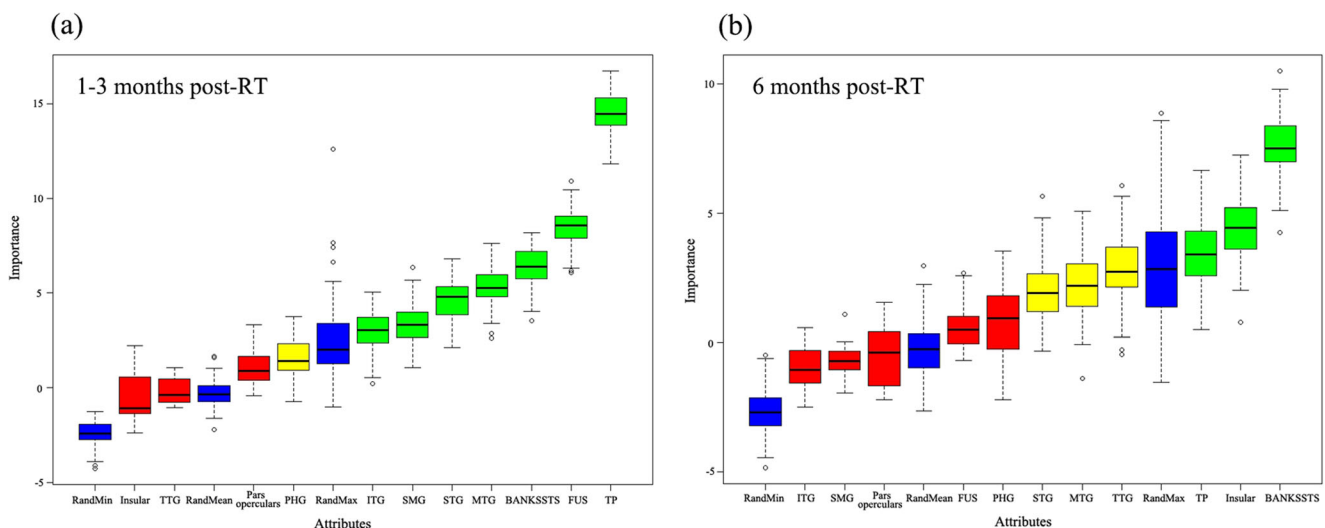


Fig. 4 Feature selection using the Boruta package. The green bars represent important attributes, the red bars represent unimportant attributes, and the yellow bars represent attributes of uncertain importance. The WM volume alterations in the TP, FUS, BANKSSTS, MTG, STG, SMG, and ITG at 1–3 months post-RT (a), and the WM volume alterations in the BANKSSTS, insular gyrus, and TP at 6 months

post-RT (b) had important characteristic attributes. Abbreviations: WM, white matter; TP, temporal pole; FUS, fusiform; MTG, middle temporal gyrus; STG, superior temporal gyrus; SMG, supramarginal gyrus; ITG, inferior temporal gyrus; RT, radiotherapy; NPC, nasopharyngeal carcinoma

good predictive performance, while the model constructed by SVM had the best diagnostic performance, with an AUC value, accuracy, sensitivity, and specificity of 0.842, 0.826, 0.750, and 0.842, respectively (Table 5 and Fig. 6). The

model was verified by another independent dataset, and the AUC value, accuracy, sensitivity, and specificity were 0.773, 0.737, 0.625, and 0.818, respectively (Table 5 and Fig. 6).

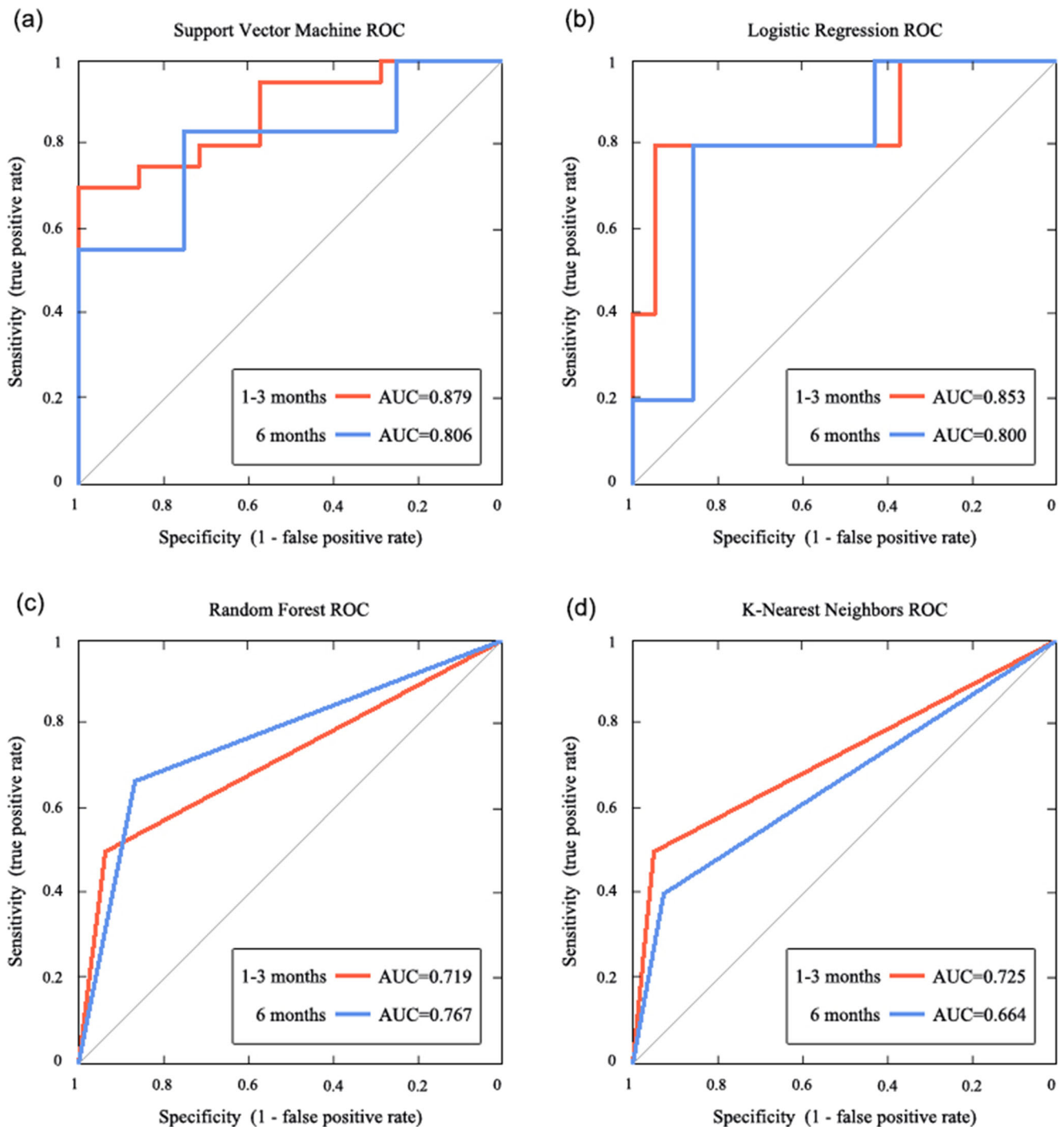


Fig. 5 ROC curves of multiple classifiers based on machine learning methods for original data with temporal WM volume alteration. The AUC values of the prediction models constructed based on SVM, LR, RF, and KNN were 0.879, 0.853, 0.719, and 0.725 at 1–3 months post-RT, respectively, and 0.806, 0.800, 0.767, and 0.664 at 6 months post-

RT, respectively. Abbreviations: ROC, receiver operating characteristic; WM, white matter; AUC, area under the curve; SVM, support vector machine; LR, logistic regression; RF, random forest; KNN, k-nearest neighbors; RT, radiotherapy.

Table 5 Predictive model constructed with absolute temporal WM volume at 1–3 months post-RT for original data had acceptable predictive efficiency for external independent verification data based on the SVM method

	Model	Testing Set				External Validation Set			
		AUC	Accuracy	Sensitivity	Specificity	AUC	Accuracy	Sensitivity	Specificity
1–3 months	SVM	0.842	0.826	0.750	0.842	0.773	0.737	0.625	0.818
	LR	0.798	0.792	0.714	0.824	0.659	0.632	0.500	0.636
	RF	0.771	0.818	0.667	0.875	0.534	0.579	0.500	0.600
	KNN	0.725	0.875	0.667	0.905	0.318	0.368	0.000	0.467

Abbreviations: *WM*, white matter; *RT*, radiotherapy; *SVM*, support vector machine; *LR*, logistic regression; *RF*, random forest; *KNN*, k-nearest neighbors; *AUC*, area under the curve

Discussion

To the best of our knowledge, this study is the first prospective study to combine quantitative MRI technology and machine learning methods to explore the predictive value of RT-related WM volumetric alterations at the early stage for RN occurrence at the late-delay stage. Although both RN and NRN patients exhibited progressive atrophy in the STG within 1-year post-RT, the patients in the RN group showed a more rapid volume decrease than those in the NRN group. Furthermore, the temporal WM volume alterations at the early stage (1–3 months and 6 months post-RT) could identify and predict RN occurrence at the late-delay stage, and the model constructed by SVM had the best diagnostic performance. Notably, the predictive model constructed with absolute temporal volume at 1–3 months post-radiotherapy also presented a similar predictive performance, which was verified by another independent dataset. Thus, temporal WM volume alterations (or absolute volume) in patients with NPC at the acute stage and early-delay stage post-RT may serve as potential biomarkers for the prediction of RN at the late-delay stage.

Although both RN and NRN patients exhibited time- and dose-dependent WM atrophy in the STG within 1-year post-RT, the RN patients had increased atrophy compared to the NRN patients. Animal experiments and clinical studies have indicated that RT-induced microvascular injury serves as a crucial pathological mechanism for RN occurrence [15, 16, 29, 30]; thus, increasing atrophy of the STG in the RN group may be attributed to more severe RT-induced vascular damage in the STG area. A histopathological study also demonstrated that the patient with NPC who developed severe temporal lobe radiation injury 5 years after irradiation had a more extensive impairment of the microcirculation, including structural changes of the vessel wall and perivascular inflammatory reaction, which resulted in complete temporal WM destruction [31]. Our findings are consistent with those of a previous

study by Zhang et al, who found that the patients who developed RN during follow-up had a more severe cortical thinning and larger cortical surface area in the STG compared to those who did not, although they also found abnormalities in other subfields of the temporal lobe [32]. These findings illustrated that the morphological alterations in the temporal regions, especially the STG, at the early stage post-RT may characterize RN at the late-delay stage. Future research is needed to combine multimodal imaging technology and pathological analysis to validate our findings and hypotheses.

Furthermore, combined with machine learning, we found that temporal WM volume alterations at the early stage (1–3 months and 6 months post-RT) in patients with NPC post-RT have a high predictive value for RN occurrence at the late-delay stage. We constructed the prediction models with both standardized temporal WM volume (divided by baseline) and absolute temporal WM volume (which is more easily obtained in clinical practice) and, interestingly, obtained similar predictive power. Moreover, the model constructed with absolute temporal WM volume was verified by an additional independent dataset. Several recent studies that used imaging before RN reported success in predicting RN in patients with NPC at the late-delay stage post-RT. Indeed, using texture features extracted from the MR images of the medial temporal lobe, GM, and WM before RN onset, Zhang et al developed predictive models for RN in patients with NPC [33]. Although they also obtained a high predictive power, they constructed predictive models with MR scans at the late-delay stage (median latency to RN: 41 months), at which stage the injury was irreversible and preventive therapy was not applicable [6, 7]. Moreover, combined with radiomics features and clinical factors, Hou et al developed and validated an MRI-based radiomics nomogram model for the early detection of RTLI in patients with NPC with texture features extracted from bilateral temporal lobes at the end of RT. The results demonstrated the potential power of radiomics features for the early prediction of RN in patients with NPC post-RT [34]. Our findings are complementary to these previous studies, which support the feasibility of temporal WM volume (alteration or

absolute) at the early stage post-RT for the early identification of RN. Compared to radiomic features, temporal volume is much easier to obtain in clinical practice; thus, our findings could predict RN occurrence more effectively and

conveniently at the early stage, which may help preventive therapy for RN [35–37].

Moreover, the prediction model combining temporal WM volume and dosimetric factor had the best prediction

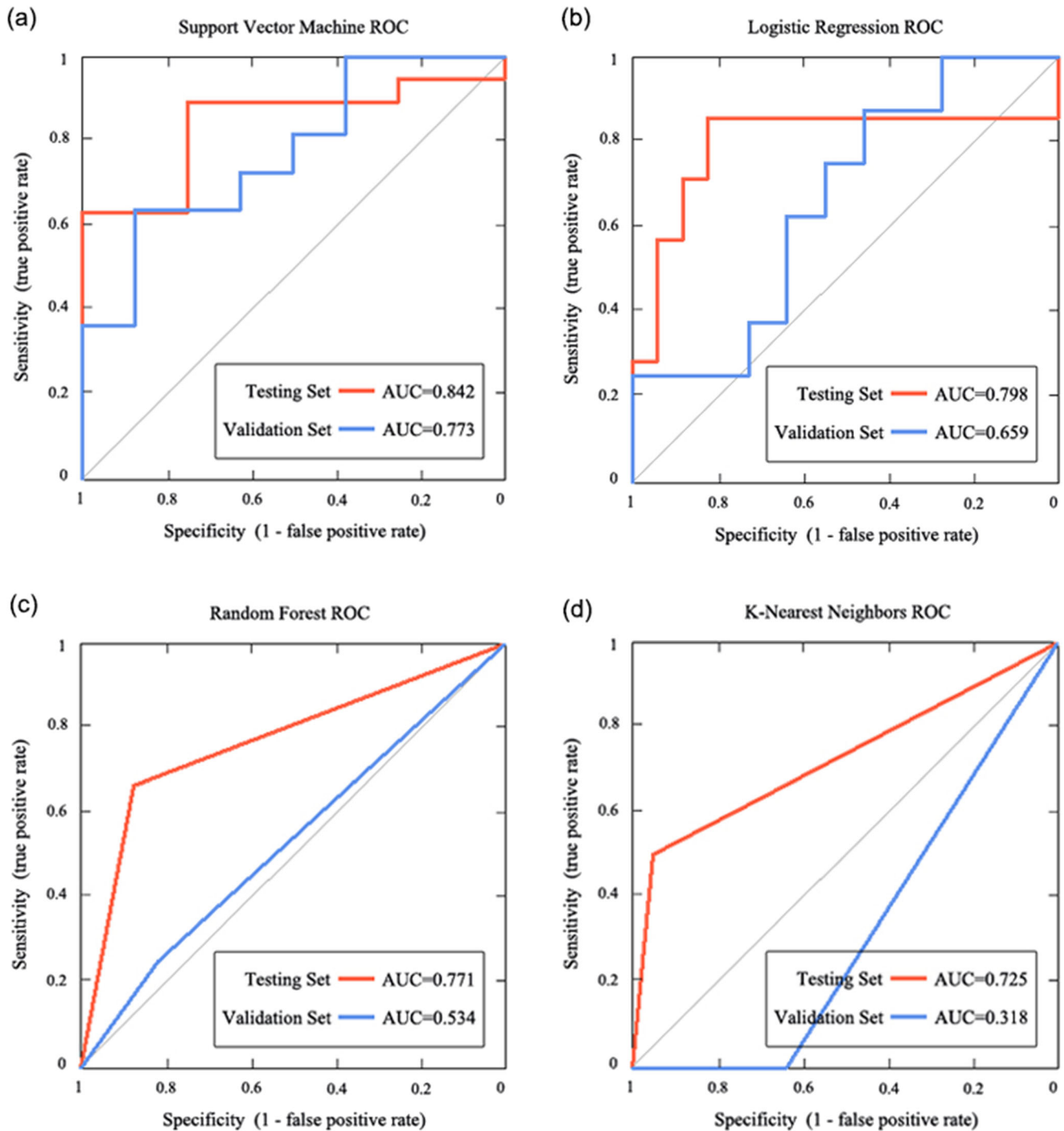


Fig. 6 ROC curves of multiple classifiers based on machine learning methods for original data and other independent verification data with absolute temporal WM volume at 1–3 months post-RT. The prediction models constructed based on SVM, LR, RF, and KNN were verified on the testing set, with AUC values of 0.842, 0.798, 0.771, and 0.725, respectively, while the prediction models constructed based on

SVM, LR, RF, and KNN were verified using an independent verification dataset, with AUC values of 0.773, 0.659, 0.534, and 0.318, respectively. Abbreviations: ROC, receiver operating characteristic; AUC, area under the curve; WM, white matter; SVM, support vector machine; LR, logistic regression; RF, random forest; KNN, k-nearest neighbors; RT, radiotherapy

performance compared to the models constructed with WM volume and dosimetric factor only, while the predictive model constructed with temporal WM only exhibited better performance than the model constructed with dosimetric factor only. The dose has been previously identified as a strong predictor of RN [38, 39], and our findings also revealed that dosimetric factors could improve the prediction performance. Moreover, our findings indicated that temporal WM volume alterations at the early stage could serve as a more important predictor than the dosimetric factor; this is unsurprising, given that the temporal WM volume alterations at the early stage attributed to both the dosimetric factor and the individuals' sensitive to dose [40–42], which had more information than dosimetric factor only.

This research has several limitations. First, the sample of the RN group was relatively small. Large-scale research is needed to verify these preliminary findings. Second, the 36-month observation period of patients post-RT lacks literature support. As a next step, we plan to extend the observation period and shorten the follow-up interval for patients with neurological symptoms in order to record the time to RN after RT more accurately. Finally, multi-modal MRI is needed to characterize the significance of brain changes (including brain structure, function, and network) for RN occurrence.

Conclusions

This is the first study to explore the predictive value for RN in patients with NPC with temporal WM volume alterations at the early stage (1–3 months and 6 months post-RT). Divergent STG atrophy trajectories were observed in patients with NPC with or without RN. Although both groups exhibited time-dependent atrophy in the STG, the patients in the RN group showed a sharper increase in atrophy compared to those in the NRN group. Furthermore, temporal WM volume alteration (or absolute volume) at the early stage could predict RN occurrence at the late-delay stage after RT. The present findings shed light on the early detection and prevention of RN in patients with NPC post-RT.

Supplementary Information The online version contains supplementary material available at <https://doi.org/10.1007/s00330-022-08907-z>.

Acknowledgements We thank LetPub (www.letpub.com) for its linguistic assistance during the preparation of this manuscript.

Funding This work has received funding by grants from the Natural Scientific Foundation of China (grant numbers: 81401399, 81560283, and 81201084), the Guangdong Basic and Applied Basic Research Foundation (2019A1515011143, 2020A1515011332, and 2022A1515012503).

Declarations

Guarantor The scientific guarantor of this publication is Yingwei Qiu.

Conflict of interest The authors of this manuscript declare no relationships with any companies, whose products or services may be related to the subject matter of the article.

Statistics and biometry One of the authors (Yingwei Qiu) has significant statistical expertise.

Informed consent Written informed consent was obtained from all subjects (patients) in this study.

Ethical approval Sun Yat-sen University Cancer Center Institutional Review Board approval was obtained.

Study subjects or cohorts overlap Sixty-one study subjects have been previously reported in our prior publication, title: Irradiation-related longitudinal white matter atrophy underlies cognitive impairment in patients with nasopharyngeal carcinoma, which is published in *Brain Imaging and Behavior* 15, 2426–2435 (2021). In our previous study, we tried to longitudinally investigate alterations in cerebral WM volume as a function of irradiation dose and time after standard radiotherapy in NPC patients. Based on our previous study, we further attempted to elucidate the divergent change trajectories of temporal WM volume in NPC patients with different outcomes (RN or no RN), and to determine whether WM volume alterations at early stage could predict RN occurrence at late-delay stage.

Methodology

- prospective
- case-control study
- performed at one institution

References

1. Torre LA, Bray F, Siegel RL, Ferlay J, Lortet-Tieulent J, Jemal A (2015) Global cancer statistics, 2012. *CA Cancer J Clin* 65:87–108
2. Wei KR, Zheng RS, Zhang SW, Liang ZH, Li ZM, Chen WQ (2017) Nasopharyngeal carcinoma incidence and mortality in China, 2013. *Chin J Cancer* 36:90
3. Lee AW, Ma BB, Ng WT, Chan AT (2015) Management of nasopharyngeal carcinoma: current practice and future perspective. *J Clin Oncol* 33:3356–3364
4. Chen YP, Chan ATC, Le QT, Blanchard P, Sun Y, Ma J (2019) Nasopharyngeal carcinoma. *Lancet* 394:64–80
5. Wu VWC, Tam SY (2020) Radiation induced temporal lobe necrosis in nasopharyngeal cancer patients after radical external beam radiotherapy. *Radiat Oncol* 15:112
6. Soussain C, Ricard D, Fike JR, Mazon JJ, Psimaras D, Delattre JY (2009) CNS complications of radiotherapy and chemotherapy. *Lancet* 374:1639–1651
7. Mao YP, Zhou GQ, Liu LZ et al (2014) Comparison of radiological and clinical features of temporal lobe necrosis in nasopharyngeal carcinoma patients treated with 2D radiotherapy or intensity-modulated radiotherapy. *Br J Cancer* 110:2633–2639
8. Zheng Z, Wang B, Zhao Q et al (2022) Research progress on mechanism and imaging of temporal lobe injury induced by radiotherapy for head and neck cancer. *Eur Radiol* 32:319–330

9. Zhao LM, Kang YF, Gao JM et al (2021) Functional connectivity density for radiation encephalopathy prediction in nasopharyngeal carcinoma. *Front Oncol* 11:687127
10. Tringale KR, Nguyen TT, Karunamuni R et al (2019) Quantitative imaging biomarkers of damage to critical memory regions are associated with post-radiation therapy memory performance in brain tumor patients. *Int J Radiat Oncol Biol Phys* 105:773–783
11. Raschke F, Wesemann T, Wahl H et al (2019) Reduced diffusion in normal appearing white matter of glioma patients following radio(chemo)therapy. *Radiother Oncol* 140:110–115
12. Yang Y, Lin X, Li J et al (2019) Aberrant brain activity at early delay stage post-radiotherapy as a biomarker for predicting neurocognitive dysfunction late-delayed in patients with nasopharyngeal carcinoma. *Front Neurol* 10:752
13. Qiu Y, Guo Z, Han L et al (2018) Network-level dysconnectivity in patients with nasopharyngeal carcinoma (NPC) early post-radiotherapy: longitudinal resting state fMRI study. *Brain Imaging Behav* 12:1279–1289
14. Lv X, He H, Yang Y et al (2019) Radiation-induced hippocampal atrophy in patients with nasopharyngeal carcinoma early after radiotherapy: a longitudinal MR-based hippocampal subfield analysis. *Brain Imaging Behav* 13:1160–1171
15. Xie Y, Huang H, Guo J, Zhou D (2018) Relative cerebral blood volume is a potential biomarker in late delayed radiation-induced brain injury. *J Magn Reson Imaging* 47:1112–1118
16. Klos J, van Laar PJ, Sinnige PF et al (2019) Quantifying effects of radiotherapy-induced microvascular injury; review of established and emerging brain MRI techniques. *Radiother Oncol* 140:41–53
17. Chapman CH, Zhu T, Nazem-Zadeh M et al (2016) Diffusion tensor imaging predicts cognitive function change following partial brain radiotherapy for low-grade and benign tumors. *Radiother Oncol* 120:234–240
18. Chen Q, Lv X, Zhang S et al (2020) Altered properties of brain white matter structural networks in patients with nasopharyngeal carcinoma after radiotherapy. *Brain Imaging Behav* 14:2745–2761
19. Guo Z, Han L, Yang Y et al (2018) Longitudinal brain structural alterations in patients with nasopharyngeal carcinoma early after radiotherapy. *Neuroimage Clin* 19:252–259
20. Liyan L, Si W, Qian W et al (2018) Diffusion Kurtosis as an in vivo imaging marker of early radiation-induced changes in radiation-induced temporal lobe necrosis in nasopharyngeal carcinoma patients. *Clin Neuroradiol* 28:413–420
21. Wu G, Luo SS, Balasubramanian PS et al (2020) Early stage markers of late delayed neurocognitive decline using diffusion kurtosis imaging of temporal lobe in nasopharyngeal carcinoma patients. *J Cancer* 11:6168–6177
22. Peiffer AM, Creer RM, Linville C et al (2014) Radiation-induced cognitive impairment and altered diffusion tensor imaging in a juvenile rat model of cranial radiotherapy. *Int J Radiat Biol* 90:799–806
23. Lin X, Tang L, Li M et al (2021) Irradiation-related longitudinal white matter atrophy underlies cognitive impairment in patients with nasopharyngeal carcinoma. *Brain Imaging Behav*. <https://doi.org/10.1007/s11682-020-00441-0>
24. Erickson BJ, Korfiatis P, Akkuz Z, Kline TL (2017) Machine learning for medical imaging. *Radiographics* 37:505–515
25. Dosenbach NU, Nardos B, Cohen AL et al (2010) Prediction of individual brain maturity using fMRI. *Science* 329:1358–1361
26. Reuter M, Schmansky NJ, Rosas HD, Fischl B (2012) Within-subject template estimation for unbiased longitudinal image analysis. *NeuroImage* 61:1402–1418
27. Steele JS (2013) Longitudinal data analysis for the behavioral sciences using R. *Structural Equation Modeling—a Multidisciplinary Journal* 20:175–180
28. Cnaan A, Laird NM, Slator P (1997) Using the general linear mixed model to analyse unbalanced repeated measures and longitudinal data. *Stat Med* 16:2349–2380
29. Balentova S, Adamkov M (2015) Molecular, cellular and functional effects of radiation-induced brain injury: a review. *Int J Mol Sci* 16:27796–27815
30. Greene-Schloesser D, Moore E, Robbins ME (2013) Molecular pathways: radiation-induced cognitive impairment. *Clin Cancer Res* 19:2294–2300
31. Koot RW, Troost D, Dingemans KP, van den Bergh Weerman MA, Bosch DA (2000) Temporal lobe destruction with microvascular dissections following irradiation for rhinopharyngeal carcinoma. *Neuropathol Appl Neurobiol* 26:473–477
32. Zhang YM, Chen MN, Yi XP et al (2018) Cortical surface area rather than cortical thickness potentially differentiates radiation encephalopathy at early stage in patients with nasopharyngeal carcinoma. *Front Neurosci* 12:599
33. Zhang B, Lian Z, Zhong L et al (2020) Machine-learning based MRI radiomics models for early detection of radiation-induced brain injury in nasopharyngeal carcinoma. *BMC Cancer* 20:502
34. Hou J, Li H, Zeng B et al (2021) MRI-based radiomics nomogram for predicting temporal lobe injury after radiotherapy in nasopharyngeal carcinoma. *Eur Radiol*. <https://doi.org/10.1007/s00330-021-08254-5>
35. Xu Y, Rong X, Hu W et al (2018) Bevacizumab monotherapy reduces radiation-induced brain necrosis in nasopharyngeal carcinoma patients: a randomized controlled trial. *Int J Radiat Oncol Biol Phys* 101:1087–1095
36. Zhang P, Cao Y, Chen S, Shao L (2021) Combination of vinpocetine and dexamethasone alleviates cognitive impairment in nasopharyngeal carcinoma patients following radiation injury. *Pharmacology* 106:37–44
37. Zhou H, Sun F, Ou M et al (2021) Prior nasal delivery of antagomiR-122 prevents radiation-induced brain injury. *Mol Ther* 29:3465–3483
38. Niyazi M, Niemierko A, Paganetti H et al (2020) Volumetric and actuarial analysis of brain necrosis in proton therapy using a novel mixture cure model. *Radiother Oncol* 142:154–161
39. McDonald MW, Linton OR, Calley CS (2015) Dose-volume relationships associated with temporal lobe radiation necrosis after skull base proton beam therapy. *Int J Radiat Oncol Biol Phys* 91:261–267
40. Wang TM, Shen GP, Chen MY et al (2019) Genome-wide association study of susceptibility loci for radiation-induced brain injury. *J Natl Cancer Inst* 111:620–628
41. Alsbeih G, El-Sebaie M, Al-Rajhi N et al (2014) Among 45 variants in 11 genes, HDM2 promoter polymorphisms emerge as new candidate biomarker associated with radiation toxicity. *3 Biotech* 4:137–148
42. Lv X, Guo Z, Tang L et al (2021) Divergent effects of irradiation on brain cortical morphology in patients with nasopharyngeal carcinoma: one-year follow-up study using structural magnetic resonance imaging. *Quant Imaging Med Surg* 11:2307–2320

Publisher's note Springer Nature remains neutral with regard to jurisdictional claims in published maps and institutional affiliations.

Springer Nature or its licensor holds exclusive rights to this article under a publishing agreement with the author(s) or other rightsholder(s); author self-archiving of the accepted manuscript version of this article is solely governed by the terms of such publishing agreement and applicable law.